ACS OMEGA

http://pubs.acs.org/journal/acsodf

Article

Efficacious Sorption Capacities for Pb(II) from Contaminated Water: A Comparative Study Using Biowaste and Its Activated Carbon as Potential Adsorbents

Bhaswati Devi,[#] Manisha Goswami,[#] Suprakash Rabha, Suravi Kalita, Hari Prasad Sarma, and Arundhuti Devi*

Cite This: *ACS Omega* 2023, 8, 15141−15151

Read Online

ACCESS | Metrics & More | Article Recommendations | Supporting Information

ABSTRACT: Heavy-metal pollution is a persevering environmental menace, which demands the necessity of its removal by green and ecofriendly adsorbents. To combat this problem, discarded plant biomass can be used as an efficient substitute. Herein, a comparative study has been highlighted for the removal of Pb^{2+} ions using *Euryale ferox* Salisbury seed coat and its activated carbon, which is prepared by a first-time-reported activating agent that is a novel and non-hazardous bioresource. The batch investigation revealed a 99.9% removal efficiency of Pb(II) by the activated carbon compared to *Euryale ferox* Salisbury seed coat, which shows only an 89.5% removal efficiency at neutral pH. The adsorption mechanism is mainly a multilayered process, which involves electrostatic, van der Waals, and hydrogen bonding interactions. The adsorption equilibrium, kinetic, and thermodynamic studies were examined for the biosorbents, which revealed the adsorption process to be feasible, spontaneous, and exothermic with both physisorption and chemisorption adsorption mechanisms. The desorption study asserted the reusability of both the biosorbents to a maximum of three cycles.

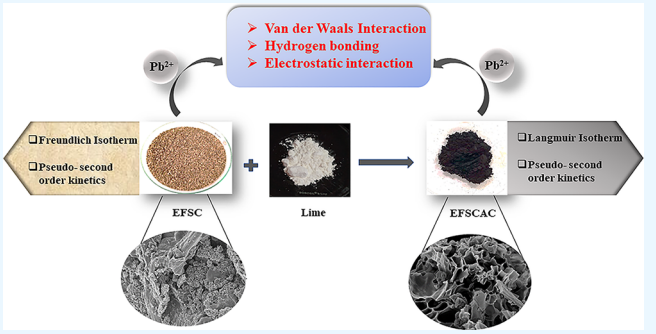

1. INTRODUCTION

Water is the centerpiece of all life forms on earth. Fresh and clean water is a must for the long span of human life. Although different industrial activities have made our life more comfortable and easier, at the same time, they are posing negative environmental impacts.[1,2] Various industrial activities produce large volumes of wastewater, which are directly or indirectly causing severe harm to our ecosystem.[3] Wastewater when disposed untreated into the surrounding environment can increase the pollution level many times more beyond the threshold limit.[4] Despite all the alleviating measures, water pollution is becoming a relentless environmental issue of the present time.[5] Heavy metal ions such as As^{3+}, Cd^{2+}, Co^{2+}, Cr^{3+}, Cu^{2+}, Ni^{2+}, Pb^{2+}, and so on produced by various industries are the major pollutants polluting our water bodies.[6−9] In living creatures, when the concentration of these metal ions exceeds the minimum tolerance limit, it can lead to their bioaccumulation in the soft tissues of living beings.[6,10,11] These heavy metal ions are even toxic at very low concentrations.[4]

Lead is one of the major heavy metal contaminants released by various industries.[5,12] Lead has been well known for its deadly effect for a long time and is also one of the most insalubrious heavy metals, which are promoters of numerous health issues. Lead poisoning may damage the vital organs and systems, which in turn affects the normal functioning of the body.[5,13] Serious exposure to lead may cause ascetic damage to the brain, liver, kidney, nervous system, and reproductive system, which may finally result in an untimely death.[4,5]

The methods used to remove heavy metal ions rely on the properties of the effluents.[4] Heavy metals are often removed using a variety of techniques, including solvent extraction, electrolysis, coagulation, reverse osmosis, chemical precipitation, ion exchange, and membrane separation.[10,11] However, all these techniques are generally expensive and have many disadvantages such as high operational cost and energy requirements, incomplete removal, the use of chemicals, and the generation of toxic and waste byproducts.[4,12,13] Therefore, there is a pressing need to create methods for reducing waste and wastewater reclamation that are both affordable and environmentally benign. The most efficient and promising alternative greener technique gaining popularity for metal ion

Received: January 9, 2023
Accepted: April 11, 2023
Published: April 20, 2023

removal is adsorption.[14−16] Adsorption processes are easy to handle, simple in design, and very cost-effective.[15] Various types of locally available low-cost adsorbents and their activated carbon have been employed for the adsorption of lead ions from contaminated wastewater.[12] Over the last decade, activated carbon has been tremendously used because of its availability, physical and chemical stability, high surface area, adsorption capacity, and porous structure.[17,18]

In this work, lead ions will be removed using a waste plant-based biomaterial and its activated carbon. The unneeded seed coat of the "Makhana" plant, scientifically known as *Euryale ferox* Salisbury, constitutes the prepared biomaterial. Available in the subtropical and tropical regions of East and Southeast India, *Euryale ferox* Salisbury is renowned for its nutritional and therapeutic benefits.[19,20] Literature reveals that different types of activated carbon has been developed using various types of chemicals as the activating agent, which is not a green and sustainable method for the preparation of activated carbon.[4] Lime, a naturally occurring, white caustic alkaline material, was used in our work as the alkali activator to obtain activated carbon from the seed coat of *Euryale ferox* (*E. ferox*). The hemicellulose, cellulose, polysaccharide, and lignin content in the carbon precursor successfully react with the activating agent, causing either pore formation, pore expansion, pore combination, or pore collapse.[17]

Thus, the study aimed to assess the adsorbing efficiency of the adsorbents generated from the seed coat of *E. ferox* and its activated carbon, which is prepared using lime as an active component. The quest for innovative green techniques for removing heavy metals has drawn our attention to the use of natural materials for developing greener low-cost techniques for treating metal-contaminated water. The chemical and physical properties of both adsorbents were determined by employing several techniques such as scanning electron microscopy (SEM), zeta potentials, BET surface area analysis, Fourier transform infrared spectroscopy (FTIR), thermal gravimetric analysis (TGA), energy-dispersive X-ray analysis (EDX), X-ray diffraction analysis (XRD), contact angle analysis and X-ray photoelectron spectroscopy (XPS). The effect of the initial concentration, pH of metal solution, contact time, and biosorbent loading were investigated. Isotherm, kinetic, and thermodynamic studies were performed to predict the feasibility and nature of the adsorption techniques.

2. EXPERIMENTAL SECTION

2.1. Materials. Fresh fruits of *E. ferox* were collected from various wetlands of North Eastern locales of which only the seed coat (an agricultural waste) is used in the experiment. A lead solution of 1 g L^{-1} was prepared using lead nitrate $Pb(NO)_3$, which is commercially procured from Sigma-Aldrich, USA. The standard calibration curves for Pb(II) were obtained by using a 1 g L^{-1} standard Pb(II) solution from Merck. Ultrapure Milli-Q water was used throughout the experiment.

2.2. Preparation of the *E. ferox* Seed Coat (EFSC) Powder and *E. ferox* Seed Coat Activated Carbon (EFSCAC). The *E. ferox* seed coats were washed, dried, and ground into powder, which were subsequently sieved in the 75−200 mm fraction range. The produced EFSC powder was repeatedly washed to produce washings that were colorless and turbidity-free, and it was then air-dried for 48 h before being oven-dried at 40 °C.

The activated carbon of EFSC was prepared using lime as the activating agent with an impregnation ratio of 1:0.66. To maintain the ratio, 10 g of lime was dispersed in 100 mL of Milli-Q water and was mechanically agitated for 30 min. The filtrate obtained served as the activating agent. An amount of 6.6 g of EFSC was soaked for 24 h in the filtrate and was subsequently stirred for another 72 h and filtered. The obtained residue was oven dried at 40 °C until it was moisture-free. The dried sample was ground into powder and then carbonized in a muffle furnace at 350 °C for 4 h to obtain the activated carbon (EFSCAC), which was thoroughly washed with 0.1 M HCl to remove the organic salts and ash. After this, EFSCAC was repeatedly rinsed with Milli-Q water until neutralization, which is followed by oven-drying at 40 °C. The dried EFSCAC was ground into powder using a mortar and pestle and was stored in a desiccator for further use.

2.3. Lead Adsorption Experiments. The adsorption efficiencies of EFSC and EFSCAC for Pb(II) were studied by carrying out batch adsorption experiments in a 100 mL Erlenmeyer flasks and kept in a thermostatic shaker. Adsorbent doses of 0.2−2 g L^{-1} of EFSC and EFSCAC were mixed in a 50 mL solution of Pb(II) (25−100 mgL^{-1}) at different pH values (4−7) and agitated at 150 rpm at different time intervals (20−240 min) and temperatures (298, 303, 308, and 313 K). The pH values of Pb(II) solutions were obtained by adding 0.1 M HCl and 0.1 M NaOH solutions.

The removal efficiency and equilibrium adsorption capacity of Pb(II) by EFSC and EFSCAC were calculated by the following equations.

$$\text{removal efficiency}(\%) = \left(\frac{C_0 - C_t}{C_0}\right) \times 100 \quad (1)$$

$$\text{equilibrium adsorption capacity, } q_e = (C_o - C_e) \times \frac{V}{W} \quad (2)$$

Here, C_o (mg L^{-1}) is the initial concentration of Pb(II) and C_t (mg L^{-1}) is the Pb(II) concentration at a pre-specified time, V (L) is the volume of Pb(II) solution, and W (mg) is the adsorbent mass.

3. RESULTS AND DISCUSSION

3.1. Characterization of EFSC and EFSCAC. *3.1.1. Structure Characterization.* A comparison between the FTIR spectra of EFSC and EFSCAC was done before and after adsorption of Pb(II) ions (Figure 1). In the FTIR spectra (a), the detectable peaks observed at wavenumbers 3381.44, 2910.65, 1735.39, 1641.25, 1516.75, and 1378.92 cm^{-1} confirm the presence of O−H stretching for water or alcohol, C−H stretching, C═O group of an aldehyde, ketone, or ester, aliphatic C═C stretching, aromatic C═C stretching, and C−H bending, respectively, while the peaks at 1253.68 and 1041.00 cm^{-1} are due to the C−O stretching and O−H bending of primary, secondary, and tertiary alcohols, esters, and ethers, which are found to be absent in the FTIR spectra (c) of EFSCAC. This finding can be attributed to the release of volatile compounds from the carbonized material.[21−24] The FTIR spectra (c) of EFSCAC shows an absorption peak at 3418.25 cm^{-1}, which reveals the presence of O−H stretching due to the adsorbed moisture on the surface of activated carbon.[23] The absorption peak at a wavenumber of 2932.76 cm^{-1} demonstrates the existence of aliphatic C−H stretching,

https://doi.org/10.1021/acsomega.3c00142
ACS Omega 2023, 8, 15141−15151

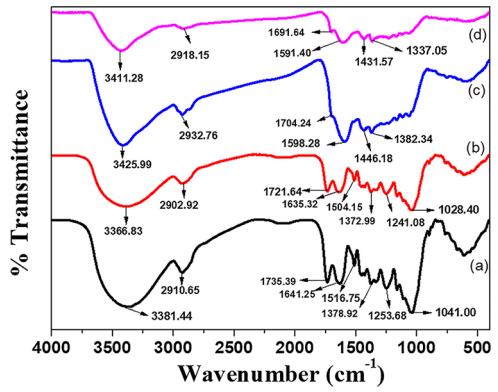

Figure 1. FTIR spectra: (a) EFSC (before adsorption), (b) EFSC (after adsorption), (c) EFSCAC (before adsorption), and (d) EFSCAC (after adsorption).

which means the presence of alkane compounds.[21] The peak at 1704.24 cm^{-1}, which is of a lower intensity, is due to the presence of an aliphatic C═C stretching and C═O group. The decreased intensity of the peak can be apparently because of the decreasing aliphaticity of EFSCAC. Due to the formation of activated carbon using lime as the activating agent, the aromatic C═C bond has been formed, which is evident from the presence of absorption peak at 1598.28 cm^{-1}. This implies the formation of aromatic compounds, which are the integral components of activated carbon.[23] The peak obtained at 1382.34 cm^{-1} with a lower intensity is for the presence of C−H bending, which indicates a decrease in aliphaticity in the activated carbon EFSCAC. All the respective absorption peaks that appeared due to EFSC (Figure 1a) and EFSCAC (Figure 1c) shifted to lower wavenumbers after adsorption of Pb^{2+} ions as shown in Figure 1b,d, respectively. This shifting of absorption peaks after biosorption of Pb^{2+} ions in contrast to before biosorption is attributed to the binding of Pb^{2+} ions to the respective functional groups present in EFSC and EFSCAC. However, the negatively charged functional groups like the carboxylate and hydroxyl groups in the biosorbents would be preferentially responsible for the binding of Pb^{2+} ions due to the presence of electrostatic attraction between them.

Thermal gravimetric analysis (TGA) study was performed under a nitrogen atmosphere where, in accordance with the TGA curve of Figure S1a, the initial weight loss from room temperature to 98 °C is due to a dehydration process. When

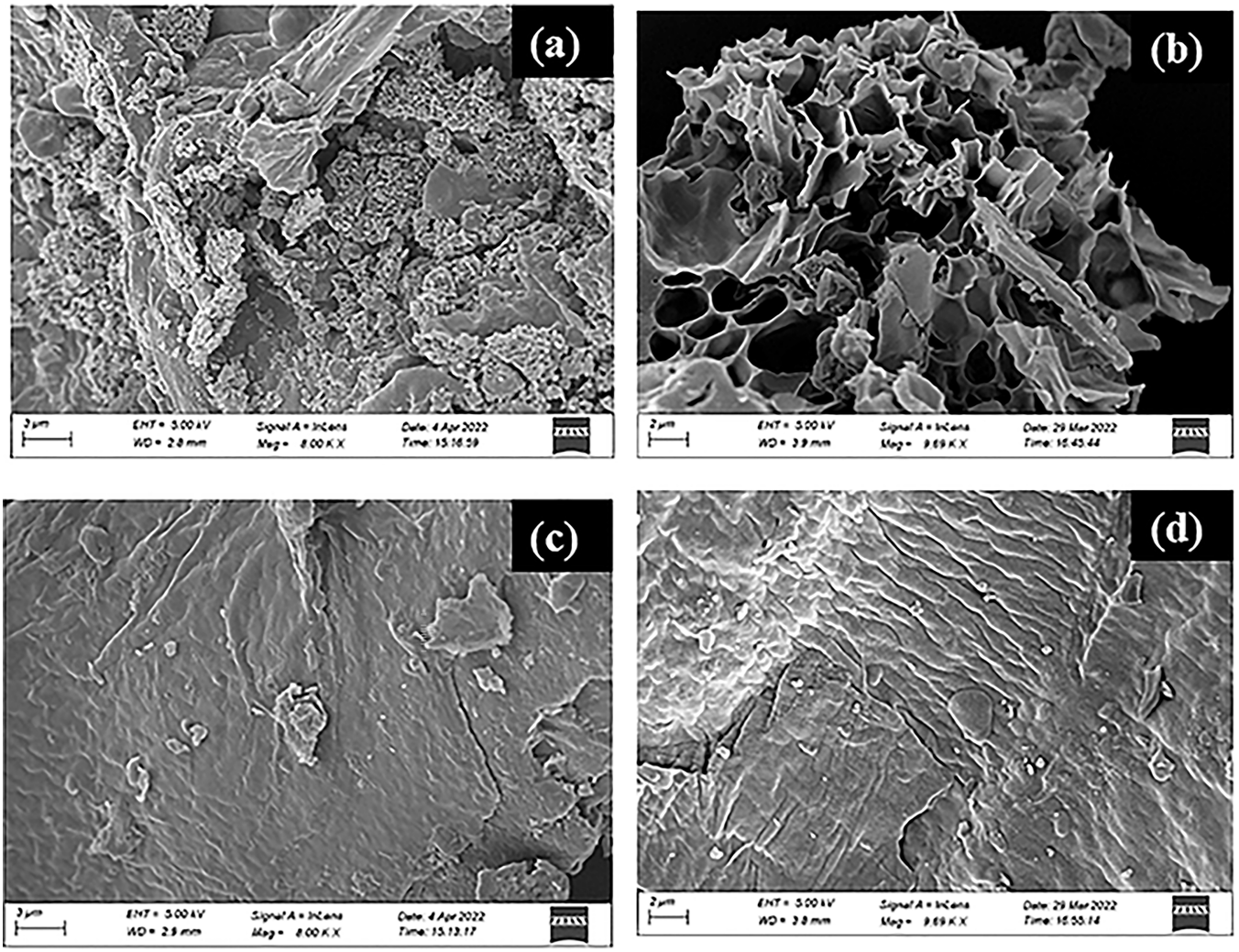

Figure 2. Scanning electron micrographs (SEM) of (a) EFSC (before adsorption), (b) EFSCAC (before adsorption), (c) EFSC (after adsorption), and (d) EFSCAC (after adsorption).

https://doi.org/10.1021/acsomega.3c00142
ACS Omega 2023, 8, 15141−15151

the temperature reached 250 °C, a weight loss of 7.35% was observed, which indicates the loss of moisture along with some small volatile matters. However, a rapid weight loss of 39.77% was observed between the temperature range of 300−370 °C, which implies the release of a CO_2 gas along with the decomposition of cellulose and hemicellulose. Another weight loss of 38.16% occurred at 370−630 °C, which contributes to the combined decomposition of hemicellulose and lignin.[24] In the TGA curve of EFSCAC Figure S1b, a preliminary mass loss of 6.41% was obtained at 300 °C, which can be attributed to the loss of moisture along with the loss of some low-molecular-weight volatile compounds. At a temperature range of 300−730 °C, a mass loss of 73% was recorded, which generally implies the decomposition of cellulose, hemicellulose, and lignin in the activated carbon.[25] However, on comparison of both Figure S1a,b, it was noted that EFSCAC was thermally more stable within the temperature range of 0−800 °C in contrast to EFSC.

Scanning electron microscopy (SEM) was performed at the same magnifications in order to investigate the surface morphology of EFSC and EFSCAC after and before adsorption of Pb^{2+} ions. The SEM images of EFSC and EFSCAC are as shown in Figure 2 to analyze the surface texture. Figure 2a shows that the surface of EFSC before adsorption is fairly smooth with some pores within it, while Figure 2b shows the highly porous surface of EFSCAC as more pores have been developed upon the activation and carbonization of EFSC. Figure 2c,d shows the SEM micrographs of EFSC and EFSCAC, respectively, after adsorption of Pb(II) ions, which reveal that the surfaces of EFSC and EFSCAC have become smooth due to the filling of pores by Pb^{2+} ions.[26] To support this information, the EDX spectra of the surface of EFSC and EFSCAC in Figure S2a,b were analyzed to confirm their elemental compositions, which show the presence of Pb^{2+} ions in the biosorbents after adsorption. An increase in the porosity further increased the surface area of EFSCAC, which is proved by BET analysis. The BET result showed that the modified EFSCAC adsorbent has a surface area of 745.77 m^2g^{-1} and which is higher in comparison to the surface area of modified and unmodified activated carbon prepared from a groundnut shell and palm kernel shell.[27,28]

From the CHNSO analysis of EFSC and EFSCAC, it was found that the carbon content of EFSCAC increased to 69.669%, whereas the carbon content of EFSC was found to be 40.836%. The hydrogen, oxygen, and nitrogen contents in EFSCAC also decrease from 5.688 to 3.450%, 44.368 to 18.584%, and 6.373 to 3.786%, respectively, compared to EFSC. The increase in the carbon content and decrease in the hydrogen, oxygen, and nitrogen contents in EFSCAC can be inferred from the release of volatile compounds from EFSC and leaving behind the carbonaceous compound.[29]

The surface charges for EFSC and EFSCAC were analyzed by performing a zeta potential within a pH range from 2 to 9 where the surface charge for both the biosorbents was found to be positive for pH 2 and negative for the pH range of 3−9 (Figure S3). The negative zeta potential charge may be due to the availability of carboxylates and phenolic hydroxyl functional groups.[30] The negative surface charge of biosorbents facilitates the adsorption of heavy metals.[31] Thus, it can be inferred that the adsorption of Pb^{2+} ions on the surface of EFSC and EFSCAC is basically because of the electrostatic attraction of the Pb^{2+} ions with negatively charged functional groups present in the biosorbents.

The XRD pattern of precursor material EFSC and the prepared activated carbon EFSCAC at 350 °C and a 1:0.66 impregnation ratio were recorded and are depicted in Figure S4. The crystalline fraction of cellulose was identified in the XRD pattern of EFSC (Figure S4a) by the sharp peak at 2θ = 22.5, while the amorphous part, which includes cellulose, hemicellulose, and lignin was identified by a sharp peak at approximately 2θ = 16.5. The presence of an amorphous structure in EFSCAC is revealed by the presence of a broad peak at 2θ = 22.08 and a lack of sharp peaks in the XRD pattern of EFSCAC (Figure S4), which highlighted the primarily amorphous structure of EFSCAC. The presence of a broad peak in EFSCAC is evidence of the emergence of a carbonaceous crystalline structure, which is a beneficial characteristic for the well-defined adsorbents.[26,32]

The contact angle of EFSCAC and EFSC is demonstrated in Figure S5, which shows the contact angle of EFSC to be 101.57° (Figure S5a), while the contact angle of EFSCAC was found to 132.08° (Figure S5b). The study reveals the more hydrophobic nature of EFSCAC as compared to EFSC due to the presence of a predominant carbonaceous crystalline structure.[33−35]

In order to comprehend the adsorption of Pb(II) ions, the wide scan and C 1s and O 1s XPS spectra for EFSC and EFSCAC were recorded. From the wide-scan spectra, after adsorption (Figures S6a and S7a), a peak for the presence of Pb(II) was obtained for both EFSC and EFSCAC, which confirmed the efficacious adsorption of Pb(II) ions by both the biosorbents. The binding energies for Pb4f were found to be 138.84 and 143.65 eV for EFSC (Figure S6b), while 138.92 and 143.69 eV for EFSCAC (Figure S7b). The C 1s peaks for EFSC (Figure S6c) appeared at 284.83 eV (C−C/C═C), 286.44 eV (C═O), and 286.95 eV (C═O), which got shifted to 284.78, 286.31, and 288.04 eV, respectively after adsorption of Pb(II) ions.[36,37] Meanwhile, for EFSCAC, the C 1s peak (Figure S7c) appeared at 284.64 eV (C−C/C═C), which, after the adsorption of Pb(II), did not get shifted, while the C 1s peaks appeared at 285.46 eV (C−O) and 287.08 eV (C═O) got shifted to 285.55 and 287.29 eV, respectively.[37] Upon the evaluation of the deconvoluted O 1s spectra of EFSC (Figure S6d), the O 1s peaks appeared at 533.03 eV (O−C═O) and 532.77 eV (C−O), which, upon adsorption, shifted to 532.68 and 533.12 eV, respectively.[38] For EFSCAC, the O 1s peaks appeared at 531.70 eV (C═O) and 533.43 eV (C−O), which got relocated to 531.76 and 533.31 eV after adsorption of Pb(II) ions (Figure S7d).[36] Thus, it is affirmed that the presence of active groups such as C−O, C═O, or O−C═O in both the biosorbents EFSC and EFSCAC is involved in the stable complex formation with the Pb(II) ions, which consequently results in the effective removal of Pb(II) ions from contaminated water.[39]

3.2. Effect of Various Parameters on Adsorption.

3.2.1. Effect of the pH. The pH affects the efficiency of the adsorption at the solid−liquid surface. The removal of Pb(II) is analyzed as a function of pH in the range of 4−7.[40] At a basic pH, the formation of a precipitate was observed, and as such, the experiment was stopped at pH 7. As the acidity of the solution increases, the competition for the active sites between the hydrogen ions and metal ions also increases, which thereby protonates the carboxylate and the phenolic hydroxyl groups of the biosorbent surface, leading to electrostatic repulsion between the surface of the biosorbent and the Pb^{2+} ions.[41,42] Thus, when the pH is lower, the surface of the biosorbents

https://doi.org/10.1021/acsomega.3c00142
ACS Omega 2023, 8, 15141−15151

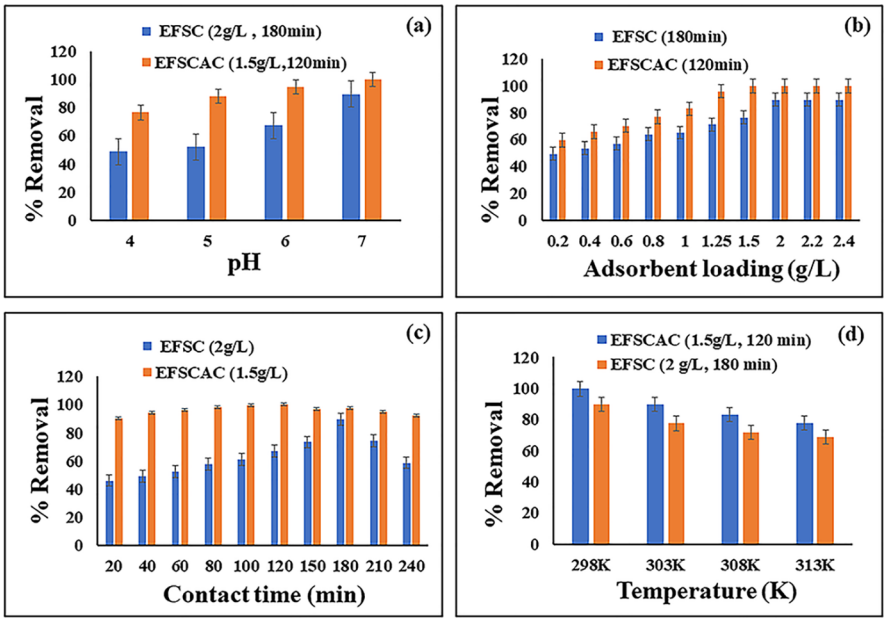

Figure 3. Effect of the (a) pH, (b) biosorbent loading, (c) contact time, and (d) temperature on the adsorption of Pb(II) by EFSC and EFSCAC.

become positively charged, which results in decreased adsorption of Pb(II) on the surface of biosorbent while the adsorption was found to increase gradually for EFSC and EFSCAC as the pH increases from 5−7 (Figure 3a).

3.2.2. Effect of Adsorbent Loading. As exhibited in Figure 3b, with the increased biosorbent loading, the removal efficiency increases while the adsorption capacity decreases. The increase in availability of adsorption sites with an increase in the biosorbent loading may be inferred to an increased removal efficacy of Pb(II). The adsorption competency decrease with a gradual increase in the biosorbent loading can be because of the unsaturation of the adsorption sites during the adsorption.[43,44]

3.2.3. Effect of the Contact Time. The investigation on the dependency of the contact time with regard to the initial concentration of Pb(II) revealed that, when the contact time of the biosorbent increases, the adsorption capacity increases (Figure 3c). Moreover, it was also found that, with the increase in the Pb(II) concentration, there is a gradual increase in the equilibrium adsorption time, which can be explained by the presence of a larger amount of the lead ion that takes more time to reach the biosorbent surface.

3.2.4. Effect of the Temperature. The effect of temperature on the adsorption of metal ions is important for the energy-dependent mechanism.[45] As found in Figure 3d, the adsorption of Pb(II) by EFSC and EFSCAC is found to be favored at lower temperatures, while, with the increase in the temperature of the solution, desorption of Pb(II) takes place, which suggests weak Van der Waals attraction between Pb(II) and the biosorbent surface, that is, physisorption.[46] As the temperature of the solution increases, the Pb(II) ions tend to escape from the biosorbents' surfaces to the liquid phase, which leads to a decrease in the thickness of the boundary layer and contributes to the exothermic nature of the adsorption process.[47] Thus, the optimized temperature for EFSC and EFSCAC is 298 K at the concentration range from 25 to 100 ppm.

3.2.5. Effect of the Ionic Strength. The effect of the ionic strength was investigated on the adsorption of Pb(II) ions using three different concentrations of NaCl solution (0.001, 0.1, and 0.5 N). The findings revealed no change in the adsorption capacity of Pb(II) for both EFSC and EFSCAC with 0.001 N NaCl, while a decrease in the adsorption capacity of Pb(II) was observed with a gradual increase in the concentration of NaCl. The reason for a decreased adsorption capacity could be due to the screening of the negative surface charges by the electrolyte ions.[48] This can be implied to the decrease in the negative surface charge with the increase in the ionic strength, which consequently results in the decreased adsorption of Pb(II) ions.

Many researchers have studied the adsorption capacity of various adsorbents in the adsorption of Pb(II), but EFSC and EFSCAC have been proved to have a better adsorption capacity for Pb(II) in comparison to many other adsorbents found in the literature (Table 1).

3.3. Adsorption Kinetic Studies. The kinetic study for the adsorption of Pb(II) by EFSC and EFSCAC was premeditated based on the variation of the contact time ranging from 20 to 240 min for a 100 ppm Pb(II) concentration. The study revealed that the equilibrium contact time for EFSC is 180 min, while EFSCAC reaches equilibrium in 120 min, which can be attributed to the fact that the adsorption rate of EFSCAC is higher than that of EFSC. To decipher the mechanism controlling the adsorption process, pseudo-first order, pseudo-second order, Elovich, intraparticle diffusion, and film diffusion models have been substantially applied. Table 2 demonstrates the correlation coefficients and other parameters obtained by executing the various kinetic models.

The pseudo-first-order kinetics proposed by Lagergren is widely executed to interpret the adsorbate−adsorbent interaction in the liquid phase, while the pseudo-second-order kinetic model assumes the mechanism of adsorption to be primarily based upon chemisorption.[49,50]

Though both the kinetic models show good correlation coefficient (R^2) values for both EFSC and EFSCAC, the experimental q_e values for the pseudo-first-order kinetic model are not in good agreement with calculated q_e values. Hence, on

https://doi.org/10.1021/acsomega.3c00142
ACS Omega 2023, 8, 15141−15151

Table 1. Maximum Adsorption Capacities of Various Biosorbents Found from the Literature

biosorbents	maximum adsorption capacity (mg g^{-1})	references
pistachio-wood waste activated carbon	190.2	39
coconut-shell activated carbon	17.193	40
chestnut-shell activated carbon	138.9	41
Enteromorpha prolifera activated carbon	146.85	42
sawdust activated carbon	200.00	43
bagasse-pith activated carbon	200.00	44
coir-pith waste activated carbon	263.00	45
E. rigida activated carbon	279.72	36
peanut-shell activated carbon	152.91	46
whole-corncob activated carbon	154.36	47
flax-shive activated carbon	147.10	48
Polygonum orientale Linn activated carbon	98.39	49
red mud	88.2	50
Turkish low-rank coal	13.58	51
crushed concrete fines	37	52
EFSC	245.61	this study
EFSCAC	298.29	this study

Table 2. Kinetic Model Parameter Values for the Adsorption of 100 ppm Pb^{2+} Ions at an Optimized Temperature of 298 K and pH 7

kinetic models and parameters		EFSC	EFSCAC
pseudo-first order	q_e (mg g^{-1})	27.829	16.707
	k_1 (min^{-1})	0.007	0.036
	R^2	0.958	0.9552
pseudo-second order	q_e (mg g^{-1})	40.983	68.027
	k_2 (min^{-1})	255×10^{-5}	0.005
	R^2	0.971	0.999
Elovich	α (mg g^{-1} min^{-1})	19.310	9.39×10^{29}
	β (g mg^{-1})	0.150	0.262
	R^2	0.870	0.995
intraparticle diffusion	intercept	13.478	55.451
	k_p (mg g^{-1} $min^{-0.5}$)	1.790	1.112
	R^2	0.952	0.991
film diffusion	intercept	0.475	1.383
	k_{id} (min^{-1})	0.007	0.036
	R^2	0.958	0.955

the basis of a good correlation between calculated and experimental q_e values, it can be implied that adsorption of Pb(II) by EFSC and EFSCAC follows a pseudo-second-order kinetic model (Figure 4c,d), which involves a chemisorption adsorption mechanism as the rate-determining step.[51−54] The basic mechanism behind the chemisorption adsorption could be hydrogen bonding or an electrostatic force of attraction and Van der Waals force of attraction.[55]

The Elovich model is executed for EFSC and EFSCAC (Figure S8a,b), which shows the correlation coefficient (R^2) to be close to unity (Table 2). The model suggests a chemisorption adsorption mechanism of Pb(II) onto the heterogeneous surface of the biosorbents.[52,56,57]

The intraparticle diffusion model has also been employed to describe the adsorption mechanism between the Pb^{2+} ions and the biosorbents (Figure 4e,f) where it is assumed that a mass transfer takes place within the pores of the adsorbent.[58] Since the plots did not pass through the origin, certain values for C are obtained, which depicts that it is not only intraparticle diffusion that solely controls the overall adsorption kinetics but there is also some other mechanism that is involved.[52] Conclusively, it can be suggested that film diffusion controls the initial rate of adsorption, while intraparticle diffusion is responsible for the second stage of the rate-controlling mechanism.[50]

The liquid film diffusion model of the adsorption mechanism was employed in this study (Figure S8c,d) to examine the role of Pb^{2+} ions that are transferred from the liquid phase to the solid surface of biosorbents used.[58] Since the plot does not pass through the origin and has some sort of value of an intercept, this suggests the presence of a thickness in the boundary layer.[52,59] Hence, it can be ascertained that the kinetics of the overall adsorption mechanism is dependent on the shift of Pb^{2+} ions from the bulk solution to the solid-phase boundary of EFSC and EFSCAC.[52]

3.4. Adsorption Isotherm Studies. The adsorption isotherm of EFSC and EFSCAC for the adsorption of Pb(II) was investigated at the equilibrium to describe the interaction between the adsorbent and adsorbate. The isotherms are represented as a function of the equilibrium adsorption capacity, q_e versus the equilibrium concentration, C_e at four different temperatures (298, 303, 308, and 313 K). To evaluate the adsorption mechanism process, Langmuir, Freundlich, and Dubinin−Radushkevich (DR) isotherm models were chosen. Table S1 shows correlation coefficients and other parameters gathered from the isotherm models. Based on the correlation coefficient (R^2), it can be inferred that EFSC preferentially follows a Freundlich isotherm while EFSCAC follows the Langmuir isotherm model for the adsorption of Pb(II).

The Langmuir isotherm model elucidates monolayer adsorption, which assumes that there is no interaction between the adsorbed molecules and all sites are equivalent.[49,60] The Langmuir isotherm for EFSC and EFSCAC is executed at four different temperatures (298, 303, 308, and 313 K), which are depicted in Figure 5a,b, respectively.

A dimensionless separation parameter, R_L is employed to explicate the viability of the adsorption mechanism, which is given by eq 3

$$R_L = \frac{1}{1 + K_L C_0} \tag{3}$$

where the K_L is the Langmuir constant and R_L indicates the shape of the isotherm, that is, unfavorable for $R_L > 1$, linear for $R_L = 1$, favorable for $0 < R_L < 1$, and irreversible for $R_L = 0$.[50,52] The R_L values for EFSC and EFSCAC lie within the range $0 < R_L < 1$ (Table S1), which indicates a favorable interaction between the biosorbents and the Pb(II) in an aqueous medium.

The Freundlich adsorption isotherm can be employed to mark out the multilayer adsorption over heterogeneous surfaces.[60,61] K_f {mg g^{-1}(L $mg^{-1})^{1/nf}$} and n are Freundlich constants and are determined from the plot of $\log q_e$ versus $\log C_e$ (Figure 5c,d) at four different temperatures (298, 303, 308, and 313 K). K_f elucidates the bond strength, while n depicts the bond energy between the adsorbate and the adsorbent. The K_f values for EFSC and EFSCAC were found to be in the range of 19.319−8.092 and 797.443−11.114, whereas the n values were in the range 2.995−2.459 and 2.371−1.871, respectively (Table S1). The values of n are

https://doi.org/10.1021/acsomega.3c00142
ACS Omega 2023, 8, 15141−15151

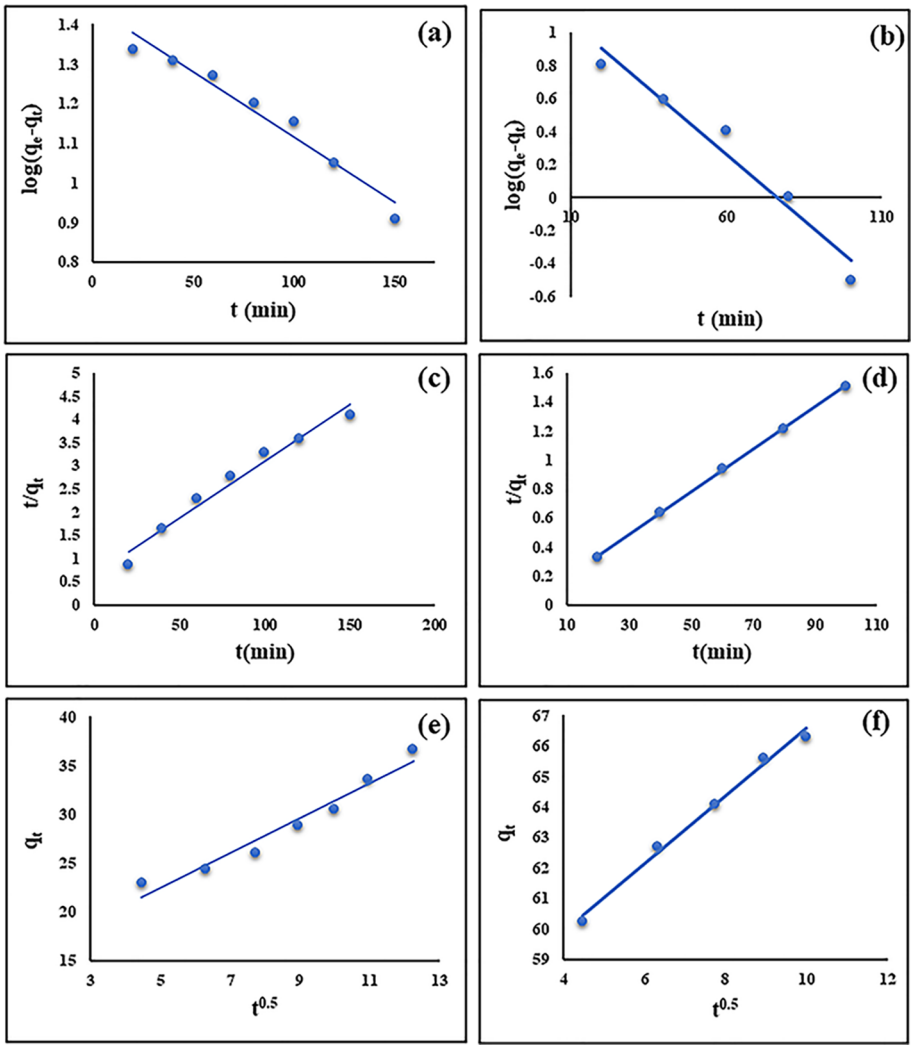

Figure 4. Pseudo-first-order model for (a) EFSC and (b) EFSCAC; pseudo-second-order model for (c) EFSC and (d) EFSCAC; intraparticle diffusion model for (e) EFSC and (f) EFSCAC.

found to be greater than 1, which depicts an effective interaction between the adsorbate and adsorbent.[60]

The Dubinin−Radushkevich (D-R) isotherm curve interprets the porous structure of the adsorbent, which predicts that the energy of adsorption is homogeneous throughout the adsorption of the adsorbate molecules.[62,63] The mean free energy, E obtained from the D-R isotherm elucidates the process of biosorption as follows.[50,60]

mean free energy value → process of biosorption

$E < 8.0$ kJ mol^{-1} → physisorption

$E = 8.0 - 16.0$ kJ mol^{-1} → ion exchange

$E > 16.0 - 400$ kJ mol^{-1} → chemisorption

The D-R isotherm for EFSC and EFSCAC is executed at four different temperatures (298, 303, 308, and 313 K), which is displayed in Figure 5e,f. Since the mean free energy value for both EFSC and EFSCAC lies in the category of $E < 8.0$ kJ mol^{-1} (Table S1), the biosorption of Pb(II) on both the biosorbents can be inferred to be physisorption.[60]

3.5. Adsorption Thermodynamics. The evaluation of adsorption thermodynamics is accomplished at different temperatures (298, 303, 308, and 313 K) by computing the thermodynamic parameters such as ΔH^0, ΔS^0, and ΔG^0 to figure out the feasibility of adsorption of Pb^{2+} ions by EFSC and EFSCAC (Figure S9a,b). The thermodynamic parameters can be resolved from the van't Hoff equation as follows:[64,65]

$$\ln K_0 = -\frac{\Delta H^0}{RT} + \frac{\Delta S^0}{R} \quad (4)$$

$$K_0 = \text{Langmuir constant } (K_L) \times 1000 \times \text{molecular weight of the adsorbate} \quad (5)$$

Here, ΔH^0 is the standard change in enthalpy, ΔS^0 is the standard change in entropy, K_0 is the equilibrium constant, T is the temperature in Kelvin, and R is the universal gas constant.

The thermodynamic parameters ΔH^0 and ΔS^0 are obtained from the intercept and slope of the plot of $\ln K_0$ versus $1/T$ (Figure S9), whereas the standard change in the Gibb's free energy, ΔG^0 for all the temperatures is obtained from the following equation:

$$\Delta G^0 = \Delta H^0 - T\Delta S^0 \quad (6)$$

Table 3 demonstrates that the ΔH^0 and ΔG^0 values are negative, which inferred that the adsorption process is

https://doi.org/10.1021/acsomega.3c00142
ACS Omega 2023, 8, 15141−15151

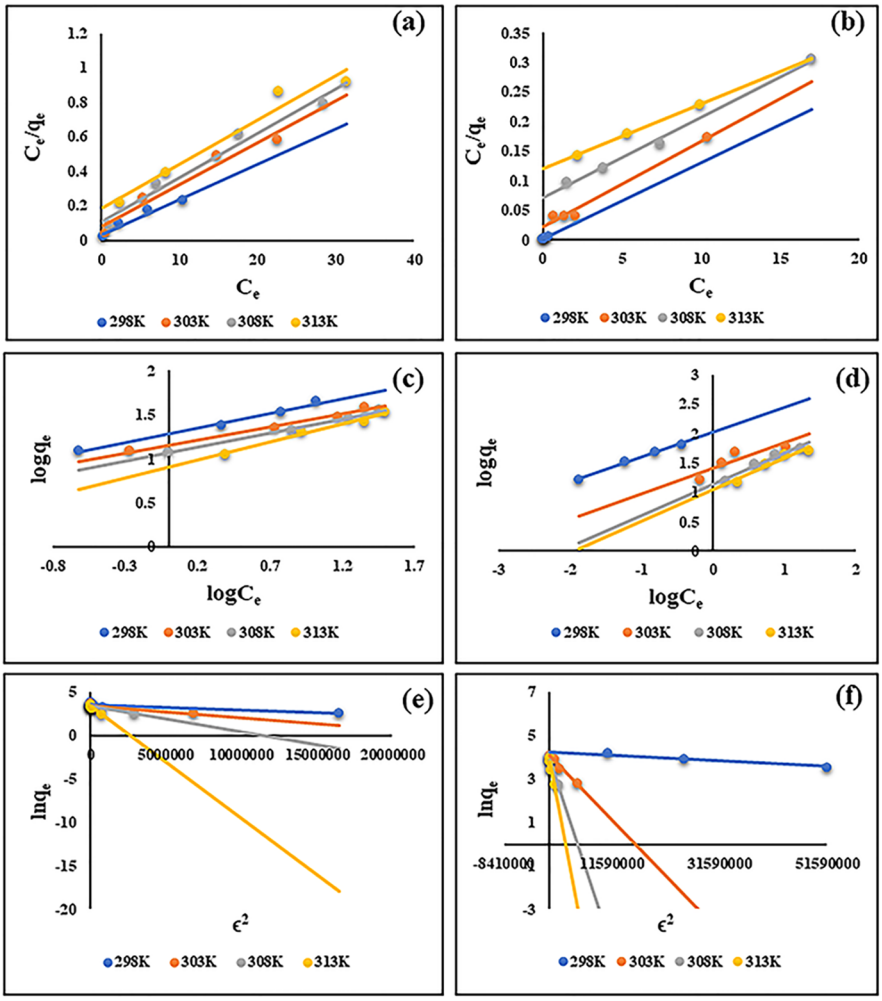

Figure 5. Langmuir isotherm for (a) EFSC and (b) EFSCAC; Freundlich isotherm for (c) EFSC and (d) EFSCAC; D-R isotherm for (e) EFSC and (f) EFSCAC.

Table 3. Thermodynamic Parameter Values for the Adsorption of Pb^{2+} Ions

biosorbents	T (K)	ΔG (kJ mol^{-1})	ΔH (kJ mol^{-1})	ΔS (kJ mol^{-1} K^{-1})
EFSC	298	−86.794	−100.063	−0.04453
	303	−86.571		
	308	−86.348		
	313	−86.126		
EFSCAC	298	−81.507	−586.726	−1.69536
	303	−73.030		
	308	−64.553		
	313	−56.076		

spontaneous, exothermic, and thermodynamically feasible. Moreover, a decrease in the negative value of ΔG^0 with an increase in the temperature realizes the diminishing spontaneity of adsorption of Pb^{2+} ions by EFSC and EFSCAC at an elevated temperature range.[63] According to the literature, when ΔG^0 values lie within the range of −20 to 0 kJ mol^{-1}, it implies physisorption, while the values in the range of −80 to −400 kJ mol^{-1} implies chemisorption.[64,65] In this study, the ΔG^0 values lie in the range of −86.794 to −86.126 kJ mol^{-1} for EFSC, while within the range of −81.507 to −56.076 kJ mol^{-1} for EFSCAC, which infers that the adsorption mechanism of Pb^{2+} ions by EFSC is chemisorption while EFSCAC follows both physisorption and chemisorption adsorption mechanisms. Moreover, the negative value of ΔS^0 (Table 3) is physisorption that can be attributed to the diminishing randomness at the adsorbate−adsorbent interface for both EFSC and EFSCAC.[52]

3.6. Desorption Studies. The desorption process after adsorption of the metals by the adsorbent helps in the recovery of valuable metals and regeneration of both the biomaterial and the activated carbon. Desorption of lead from both EFSC and EFSCAC was attempted using hydrochloric acid (HCl) of various strengths. The Pb(II)-loaded EFSC and EFSCAC were stirred with 100 mL of HCl of strengths of 0.1, 0.5, 0.75, and 1.0 M for 3 h in the case of EFSC and 2 h in the case of EFSCAC. The desorbed Pb(II) present in acid solution was analyzed using AAS. The percentage recovery of Pb(II) from EFSC was 85.0, 92.7, 95.5, and 99.5% by 0.1, 0.5, 0.75, and 1.0 M HCl, respectively. In the case of EFSCAC, corresponding values were 82.2, 88.3, 91.7, and 96.8%. Both the adsorbent could be used efficiently for three cycles and the efficiency decreases from the next cycles. The efficiency of HCl solution is because of the H^+ attack combination, which initiates displacement and converts the Pb(II) species to form chlorocompounds.

https://doi.org/10.1021/acsomega.3c00142
ACS Omega 2023, 8, 15141−15151

4. CONCLUSIONS

The study accentuates the preparation of an efficient, green, and low-cost activated carbon (EFSCAC) from the discarded seed coat of *E. ferox* (EFSC) using "lime", which is a non-toxic and edible activating agent. The performance of the competitive batch adsorption experimental process for the adsorption of Pb(II) on EFSC and EFSCAC revealed that the prepared activated carbon (EFSCAC) is a better and more efficient biosorbent for the adsorption of Pb(II) with 99.9% removal efficiency at a biosorbent dose and time of 1.5 g/L and 120 min, respectively, compared to EFSC, which shows only an 89.5% removal capacity at a higher biosorbent dose and time of 2 g/L and 180 min, respectively. The use of a lower biosorbent dose and contact time for the removal of Pb(II) from wastewater makes EFSCAC an effective and economical alternative compared to EFSC. However, the adsorption process by both the biosorbents is pH-dependent and shows better results at pH 7. The equilibrium data for both the biosorbents were analyzed by various isotherm and kinetic models that better fit the experimental equilibrium data of EFSC for the Freundlich isotherm and EFSCAC for Langmuir isotherm, whereas the pseudo-second order kinetics is followed by both the adsorbents. Thermodynamic studies of the adsorption mechanism revealed the adsorption to be exothermic accompanied by its thermodynamic feasibility, spontaneity, and decrease in randomness. Moreover, the trend of a decrease in adsorption of Pb(II) with an increasing temperature suggests that the type of adsorption is physisorption, which is also supported by the Temkin and D-R isotherms. On the other hand, chemical adsorption is supported by the Langmuir isotherm, pseudo-second order kinetics, and Elovich model from which it can be implied that adsorption of Pb(II) on EFSC and EFSCAC involves both chemisorption and physisorption simultaneously, that is, Pb(II) ions are physically adsorbed upon a unimolecular layer of chemically adsorbed Pb(II) ions. Hence, the investigation shows a very cheap and novel way of preparation of activated carbon from locally available plant biomass (EFSC) and an effective and novel activating agent, which shows far better removal efficiency of Pb(II) compared to the raw plant biomass, thus exhibiting a promising alternative for the treatment of industrial wastewater.

■ ASSOCIATED CONTENT

Supporting Information

The Supporting Information is available free of charge at https://pubs.acs.org/doi/10.1021/acsomega.3c00142.

Characterization of the adsorbents (TGA, SEM−EDX, zeta potential values, XRD, contact angle, and XPS), Elovich kinetic model, van't Hoff plot for the thermodynamic study, and isotherm model parameter values (PDF)

■ AUTHOR INFORMATION

Corresponding Author

Arundhuti Devi − *Environmental Chemistry Laboratory, Resource Management and Environment Section, Life Science Division, Institute of Advanced Study in Science and Technology, Guwahati 781035 Assam, India;* orcid.org/0000-0002-6593-7510; Email: arundhuti@iasst.gov.in; Fax: +91-361-2273062

Authors

Bhaswati Devi − *Environmental Chemistry Laboratory, Resource Management and Environment Section, Life Science Division, Institute of Advanced Study in Science and Technology, Guwahati 781035 Assam, India*

Manisha Goswami − *Environmental Chemistry Laboratory, Resource Management and Environment Section, Life Science Division, Institute of Advanced Study in Science and Technology, Guwahati 781035 Assam, India*

Suprakash Rabha − *Environmental Chemistry Laboratory, Resource Management and Environment Section, Life Science Division, Institute of Advanced Study in Science and Technology, Guwahati 781035 Assam, India*

Suravi Kalita − *Environmental Chemistry Laboratory, Resource Management and Environment Section, Life Science Division, Institute of Advanced Study in Science and Technology, Guwahati 781035 Assam, India; Homi Bhabha Centre for Science Education, Tata Institute of Fundamental Research, Mumbai 400088 Maharashtra, India*

Hari Prasad Sarma − *Department of Environmental Science, Gauhati University, Guwahati 781014 Assam, India*

Complete contact information is available at: https://pubs.acs.org/10.1021/acsomega.3c00142

Author Contributions

#B.D. and M.G. have equal contribution.

Author Contributions

B.D. contributed in conceptualization, investigation, visualization, writing and review and editing. M.G. participated in conceptualization, investigation, visualization, writing, and review and editing. S.R. contributed in the investigation. S.K. contributed in review and editing. H.P.S. conducted supervision. A.D. participated in conceptualization, writing, review, editing, and supervision.

Funding

This work was funded by Department of Science and Technology (DST), Govt. of India (no. SR/WOS-A/EA-11/2019(G)).

Notes

The authors declare no competing financial interest.

■ ACKNOWLEDGMENTS

The authors offer their sincere thanks to the Department of Science and Technology (DST), Government of India, for providing financial support in execution of the work. The authors also thank the Sophisticated Analytical Instrumentation Centre (SAIC), Institute of Advanced Study in Science and Technology (IASST), Guwahati (under the Department of Science and Technology, Government of India), for providing instrumental facilities.

■ ABBREVIATIONS

EFSC	*E. ferox* seed coat
EFSCAC	*E. ferox* seed coat activated carbon
C_0	initial concentration
C_t	concentration at pre-specified time
q_e	equilibrium adsorption capacity
V	volume of solution
M	mass of adsorbent
q_t	adsorption capacity at any time
C_e	equilibrium concentration
q_0	maximum monolayer adsorption capacity

https://doi.org/10.1021/acsomega.3c00142
ACS Omega 2023, 8, 15141−15151

K_L	Langmuir constant
R_L	dimensionless separation parameter
K_f	Freundlich constant
K_{DR}	energy of biosorption
q_m	maximum monolayer adsorption capacity
E	mean free energy
k_1	pseudo-first-order rate constant
k_2	pseudo-second-order rate constant
α	initial sorption rate
β	desorption constant
K_p	intraparticle diffusion rate constant
C	boundary layer thickness constant
k_{id}	adsorption rate constant
K_0	equilibrium constant
ΔH^0	standard change in enthalpy
ΔS^0	standard change in entropy
ΔG^0	standard change in the Gibb's free energy

REFERENCES

(1) Kırbıyık, Ç.; Pütün, A. E.; Pütün, E. Comparative studies on adsorptive removal of heavy metal ions by biosorbent, bio-char and activated carbon obtained from low cost agro-residue. *Water Sci. Technol.* **2016**, *73*, 423−436.

(2) Al-Othman, Z. A.; Ali, R.; Naushad, M. Hexavalent chromium removal from aqueous medium by activated carbon prepared from peanut shell: adsorption kinetics, equilibrium and thermodynamic studies. *Chem. Eng. J.* **2012**, *184*, 238−247.

(3) Gong, X.-Y.; Huang, Z.-H.; Zhang, H.; Liu, W.-L.; Ma, X.-H.; Xu, Z.-L.; Tang, C. Y. Novel high-flux positively charged composite membrane incorporating titanium-based MOFs for heavy metal removal. *Chem. Eng. J.* **2020**, *398*, No. 125706.

(4) Dubey, A.; Shiwani, S. Adsorption of lead using a new green material obtained from Portulaca plant. *Int. J. Environ. Sci. Technol.* **2012**, *9*, 15−20.

(5) Basu, M.; Guha, A. K.; Ray, L. Adsorption of lead on cucumber peel. *J. Cleaner Prod.* **2017**, *151*, 603−615.

(6) Wang, F.; Pan, Y.; Cai, P.; Guo, T.; Xiao, H. Single and binary adsorption of heavy metal ions from aqueous solutions using sugarcane cellulose-based adsorbent. *Bioresour. Technol.* **2017**, *241*, 482−490.

(7) Boamah, P. O.; Huang, Y.; Hua, M.; Zhang, Q.; Wu, J.; Onumah, J.; Sam-Amoah, L. K.; Boamah, P. O. Sorption of heavy metal ions onto carboxylate chitosan derivatives—a mini-review. *Ecotoxicol. Environ. Saf.* **2015**, *116*, 113−120.

(8) Fu, F.; Wang, Q. Removal of heavy metal ions from wastewaters: a review. *J. Environ. Manage.* **2011**, *92*, 407−418.

(9) Salman, M.; Athar, M.; Farooq, U. Biosorption of heavy metals from aqueous solutions using indigenous and modified lignocellulosic materials. *Rev. Environ. Sci. Bio/Technol.* **2015**, *14*, 211−228.

(10) de Moraes Rocha, G. J.; Nascimento, V. M.; Goncalves, A. R.; Silva, V. F. N.; Martín, C. Influence of mixed sugarcane bagasse samples evaluated by elemental and physical−chemical composition. *Ind. Crops Prod.* **2015**, *64*, 52−58.

(11) Pan, Y.; Cai, P.; Farmahini-Farahani, M.; Li, Y.; Hou, X.; Xiao, H. Amino-functionalized alkaline clay with cationic star-shaped polymer as adsorbents for removal of Cr (VI) in aqueous solution. *Appl. Surf. Sci.* **2016**, *385*, 333−340.

(12) Gerçel, Ö.; Gerçel, H. F. Adsorption of lead (II) ions from aqueous solutions by activated carbon prepared from biomass plant material of Euphorbia rigida. *Chem. Eng. J.* **2007**, *132*, 289−297.

(13) Ren, G.; Jin, Y.; Zhang, C.; Gu, H.; Qu, J. Characteristics of Bacillus sp. PZ-1 and its biosorption to Pb (II). *Ecotoxicol. Environ. Saf.* **2015**, *117*, 141−148.

(14) Saini, S.; Katnoria, J. K.; Kaur, I. A comparative study for removal of cadmium (II) ions using unmodified and NTA-modified Dendrocalamus strictus charcoal powder. *J. Environ. Health Sci. Eng.* **2019**, *17*, 259−272.

(15) El Malti, W.; Hijazi, A.; Abou Khalil, Z.; Yaghi, Z.; Medlej, M. K.; Reda, M. Comparative study of the elimination of copper, cadmium, and methylene blue from water by adsorption on the citrus Sinensis peel and its activated carbon. *RSC Adv.* **2022**, *12*, 10186−10197.

(16) Abilasha, D.; Lisy, L. Studies on the adsorption characteristics of Hevea Brasiliensis seed coat charcoal on Cu (II) & Zn (II) Ions. *Studies* **2016**, *1* ().

(17) Sajjadi, S. A.; Meknati, A.; Lima, E. C.; Dotto, G. L.; Mendoza-Castillo, D. I.; Anastopoulos, I.; Alakhras, F.; Unuabonah, E. I.; Singh, P.; Hosseini-Bandegharaei, A. A novel route for preparation of chemically activated carbon from pistachio wood for highly efficient Pb(II) sorption. *J. Environ. Manage.* **2019**, *236*, 34−44.

(18) Sihua, Z.; Jiwen, L.; Jiahui, S.; Guan, W.; Li, Z. A review on peach gum polysaccharide: Hydrolysis, structure, properties and applications. *Carbohydr. Polym.* **2022**, *279*, No. 119015.

(19) Kumar, A.; Jena, H. M. Preparation and characterization of high surface area activated carbon from Fox nut (Euryale ferox) shell by chemical activation with H3PO4. *Results Phys.* **2016**, *6*, 651−658.

(20) Verma, A. K.; Banerji, B.; Chakrabarty, D.; Datta, S. K. Studies on makhana (Euryale ferox Salisbury). *Curr. Sci.* **2010**, 795−800.

(21) Riyanto, C. A.; Ampri, M. S.; Martono, Y. Synthesis and Characterization of Nano Activated Carbon from Annatto Peels (Bixa orellana L.) Viewed from Temperature Activation and Impregnation Ratio of H3PO4. *EKSAKTA: J. Sci. Data Anal.* **2020**, 44−50.

(22) Ali, R.; Aslam, Z.; Shawabkeh, R. A.; Asghar, A.; Hussein, I. A. BET, FTIR, and RAMAN characterizations of activated carbon from waste oil fly ash. *Turk. J. Chem.* **2020**, *44*, 279−295.

(23) Saka, C. BET, TG−DTG, FT-IR, SEM, iodine number analysis and preparation of activated carbon from acorn shell by chemical activation with ZnCl2. *J. Anal. Appl. Pyrolysis* **2012**, *95*, 21−24.

(24) de Fatima Salgado, M.; Abioye, A. M.; Junoh, M. M.; Santos, J. A. P.; Ani, F. N. In *Preparation of activated carbon from babassu endocarpunder microwave radiation by physical activation*, IOP Conference Series: Earth and Environmental Science, IOP Publishing: 2018; p 012116. DOI: 10.1088/1755-1315/105/1/012116.

(25) Danish, M.; Hashim, R.; Ibrahim, M. M.; Sulaiman, O. Optimized preparation for large surface area activated carbon from date (Phoenix dactylifera L.) stone biomass. *Biomass Bioenergy* **2014**, *61*, 167−178.

(26) Kumar, A.; Jena, H. M. High surface area microporous activated carbons prepared from Fox nut (Euryale ferox) shell by zinc chloride activation. *Appl. Surf. Sci.* **2015**, *356*, 753−761.

(27) Eletta, A.; Tijani, I. O.; Ighalo, J. O. Adsorption of Pb (II) and phenol from wastewater using silver nitrate modified activated carbon from groundnut (Arachis hypogaea L.) shells. *West Indian J. Eng.* **2020**, *43*, 26−35.

(28) Boadu, K. O.; Joel, O. F.; Essumang, D. K.; Evbuomwan, B. O. Comparative studies of the physicochemical properties and heavy metals adsorption capacity of chemical activated carbon from palm kernel, coconut and groundnut shells. *J. Appl. Sci. Environ. Manage.* **2018**, *22*, 1833−1839.

(29) Saroha, B.; Kumar, A.; Maurya, R. R.; Lal, M.; Kumar, S.; Rajor, H. K.; Bahadur, I.; Negi, D. S. Adsorption of cysteine on metal (II) octacynaomolybdate (IV) at different pH values: Surface complexes characterization by FT-IR, SEM with EDXA, CHNS and Langmuir isotherm analysis. *J. Mol. Liq.* **2022**, *349*, No. 118197.

(30) Zacaroni, L. M.; Magriotis, Z. M.; das Graças Cardoso, M.; Santiago, W. D.; Mendonça, J. G.; Vieira, S. S.; Nelson, D. L. Natural clay and commercial activated charcoal: Properties and application for the removal of copper from cachaça. *Food Control* **2015**, *47*, 536−544.

(31) Pahlavanzadeh, H.; Motamedi, M. Adsorption of nickel, Ni (II), in aqueous solution by modified zeolite as a cation-exchange adsorbent. *J. Chem. Eng. Data* **2019**, *65*, 185−197.

(32) Prahas, D.; Kartika, Y.; Indraswati, N.; Ismadji, S. Activated carbon from jackfruit peel waste by H3PO4 chemical activation: characterization of activated carbon prepared by phosphoric acid activation of olive stones, pore structure and surface chemistry characterization. *Chem. Eng. J.* **2008**, *140*, 32−42.

https://doi.org/10.1021/acsomega.3c00142
ACS Omega 2023, 8, 15141−15151

(33) Ahmad, D.; van den Boogaert, I.; Miller, J.; Presswell, R.; Jouhara, H. Hydrophilic and hydrophobic materials and their applications. *Energy Sources, Part A* **2018**, *40*, 2686−2725.
(34) Chen, J.; Zhu, D.; Sun, C. Effect of heavy metals on the sorption of hydrophobic organic compounds to wood charcoal. *Environ. Sci. Technol.* **2007**, *41*, 2536−2541.
(35) Yu, F.; Yang, C.; Zhu, Z.; Bai, X.; Ma, J. Adsorption behavior of organic pollutants and metals on micro/nanoplastics in the aquatic environment. *Sci. Total Environ.* **2019**, *694*, No. 133643.
(36) Chen, S.; Zhu, Y.; Han, J.; Zhang, T.; Chou, R.; Liu, A.; Liu, S.; Yang, Y.; Hu, K.; Zou, L. Construction of a Molecularly Imprinted Sensor Modified with Tea Branch Biochar and Its Rapid Detection of Norfloxacin Residues in Animal-Derived Foods. *Foods* **2023**, *12*, 544.
(37) Chen, X.; Wang, X.; Fang, D. A review on C1s XPS-spectra for some kinds of carbon materials. *Fullerenes, Nanotubes, Carbon Nanostruct.* **2020**, *28*, 1048−1058.
(38) Zhao, J.; Rafat, M. N.; Yoon, C. M.; Oh, W. C. Novel Approach to Synthesis of AgZnS and TiO(2) Decorated on Reduced Graphene Oxide Ternary Nanocomposite for Hydrogen Evolution Effect of Enhanced Synergetic Factors. *Nanomaterials* **2022**, *12*, 3639.
(39) Fei, W.; Xingwen, L.; Xiao-yan, L. Selective removals of heavy metals (Pb2+, Cu2+, and Cd2+) from wastewater by gelation with alginate for effective metal recovery. *J. Hazard. Mater.* **2016**, *308*, 75−83.
(40) Doke, K. M.; Khan, E. M. Adsorption thermodynamics to clean up wastewater; critical review. *Rev. Environ. Sci. Bio/Technol.* **2013**, *12*, 25−44.
(41) Auta, M.; Hameed, B. H. Preparation of waste tea activated carbon using potassium acetate as an activating agent for adsorption of Acid Blue 25 dye. *Chem. Eng. J.* **2011**, *171*, 502−509.
(42) Aldegs, Y.; Elbarghouthi, M.; Elsheikh, A.; Walker, G. Effect of solution pH, ionic strength, and temperature on adsorption behavior of reactive dyes on activated carbon. *Dyes Pigm.* **2008**, *77*, 16−23.
(43) Vieira, M. G.; Neto, A. F.; Gimenes, M. L.; da Silva, M. G. Sorption kinetics and equilibrium for the removal of nickel ions from aqueous phase on calcined Bofe bentonite clay. *J. Hazard. Mater.* **2010**, *177*, 362−371.
(44) Aljeboree, A. M.; Alshirifi, A. N.; Alkaim, A. F. Kinetics and equilibrium study for the adsorption of textile dyes on coconut shell activated carbon. *Arabian J. Chem.* **2017**, *10*, S3381−S3393.
(45) Iamsaard, K.; Weng, C. H.; Yen, L. T.; Tzeng, J. H.; Poonpakdee, C.; Lin, Y. T. Adsorption of metal on pineapple leaf biochar: Key affecting factors, mechanism identification, and regeneration evaluation. *Bioresour. Technol.* **2022**, *344*, No. 126131.
(46) Chanzu, H. A.; Onyari, J. M.; Shiundu, P. M. Brewers' spent grain in adsorption of aqueous Congo Red and malachite Green dyes: Batch and continuous flow systems. *J. Hazard. Mater.* **2019**, *380*, No. 120897.
(47) Ren, B. N.; Wang, K. P.; Zhang, B.; Li, H.; Niu, Y.; Chen, H.; Yang, Z.; Li, X.; Zhang, H. Adsorption behavior of PAMAM dendrimers functionalized silica for Cd(II) from aqueous solution: Experimental and theoretical calculation. *J. Taiwan Inst. Chem. Eng.* **2019**, *101*, 80−91.
(48) Cynthia, A. C.; Raymond, N. Y. Aspects of kaolinite characterization and retention of Pb and Cd. *Appl. Clay Sci.* **2002**, *22*, 39−45.
(49) Mallampati, R.; Xuanjun, L.; Adin, A.; Valiyaveettil, S. Fruit Peels as Efficient Renewable Adsorbents for Removal of Dissolved Heavy Metals and Dyes from Water. *ACS Sustainable Chem. Eng.* **2015**, *3*, 1117−1124.
(50) Kumar, S.; Shahnaz, T.; Selvaraju, N.; Rajaraman, P. V. Kinetic and thermodynamic studies on biosorption of Cr(VI) on raw and chemically modified Datura stramonium fruit. *Environ. Monit. Assess.* **2020**, *192*, 248.
(51) El Haddad, M. Removal of Basic Fuchsin dye from water using mussel shell biomass waste as an adsorbent: Equilibrium, kinetics, and thermodynamics. *Journal of Taibah University for Science* **2016**, *10*, 664−674.
(52) Kalita, S.; Pathak, M.; Devi, G.; Sarma, H. P.; Bhattacharyya, K. G.; Sarma, A.; Devi, A. Utilization of Euryale ferox Salisbury seed shell for removal of basic fuchsin dye from water: equilibrium and kinetics investigation. *RSC Adv.* **2017**, *7*, 27248−27259.
(53) Gonzalez, M. H.; Araújo, G. C.; Pelizaro, C. B.; Menezes, E. A.; Lemos, S. G.; de Sousa, G. B.; Nogueira, A. R. Coconut coir as biosorbent for Cr(VI) removal from laboratory wastewater. *J. Hazard. Mater.* **2008**, *159*, 252−256.
(54) Bo, H.; Meice, L.; Dali, W.; Yiheng, S.; Li, Z. Versatile magnetic gel from peach gum polysaccharide for efficient adsorption of Pb2+ and Cd2+ ions and catalysis. *Carbohydr. Polym.* **2018**, *181*, 785−792.
(55) Ge, Y.; Li, Z. Application of Lignin and Its Derivatives in Adsorption of Heavy Metal Ions in Water: A Review. *ACS Sustainable Chem. Eng.* **2018**, *6*, 7181−7192.
(56) El-Sadaawy, M.; Abdelwahab, O. Adsorptive removal of nickel from aqueous solutions by activated carbons from doum seed (Hyphaenethebaica) coat. *Alexandria Eng. J.* **2014**, *53*, 399−408.
(57) Cheung, C. W.; Porter, J. F.; McKay, G. Elovich equation and modified second-order equation for sorption of cadmium ions onto bone char. *Journal of Chemical Technology & Biotechnology* **2000**, *75*, 963−970.
(58) Kalavathy, M. H.; Karthikeyan, T.; Rajgopal, S.; Miranda, L. R. Kinetic and isotherm studies of Cu(II) adsorption onto H3PO4-activated rubber wood sawdust. *J. Colloid Interface Sci.* **2005**, *292*, 354−362.
(59) Baruah, S.; Devi, A.; Bhattacharyya, K. G.; Sarma, A. Developing a biosorbent from Aegle Marmelos leaves for removal of methylene blue from water. *Int. J. Environ. Sci. Technol.* **2017**, *14*, 341−352.
(60) Raghav, S.; Kumar, D. Adsorption Equilibrium, Kinetics, and Thermodynamic Studies of Fluoride Adsorbed by Tetrametallic Oxide Adsorbent. *J. Chem. Eng. Data* **2018**, *63*, 1682−1697.
(61) Taiwo, A. F.; Chinyere, N. J. Sorption Characteristics for Multiple Adsorption of Heavy Metal Ions Using Activated Carbon from Nigerian Bamboo. *J. Mater. Sci. Chem. Eng.* **2016**, *04*, 39−48.
(62) Rahman, N.; Haseen, U. Equilibrium Modeling, Kinetic, and Thermodynamic Studies on Adsorption of Pb(II) by a Hybrid Inorganic−Organic Material: Polyacrylamide Zirconium(IV) Iodate. *Ind. Eng. Chem. Res.* **2014**, *53*, 8198−8207.
(63) Dada, A. O.; Olalekan, A. P.; Olatunya, A. M.; Dada, O. J. I. J. C. Langmuir, Freundlich, Temkin and Dubinin−Radushkevich Isotherms Studies of Equilibrium Sorption of Zn 2+ Unto Phosphoric Acid Modified Rice Husk. *IOSR J. Appl. Chem.* **2012**, *3*, 38−45.
(64) Liu, Y. Is the Free Energy Change of Adsorption Correctly Calculated? *J. Chem. Eng. Data* **2009**, *54*, 1981−1985.
(65) Lima, E. C.; Hosseini-Bandegharaei, A.; Moreno-Piraján, J. C.; Anastopoulos, I. A critical review of the estimation of the thermodynamic parameters on adsorption equilibria. Wrong use of equilibrium constant in the Van't Hoof equation for calculation of thermodynamic parameters of adsorption. *J. Mol. Liq.* **2019**, *273*, 425−434.

https://doi.org/10.1021/acsomega.3c00142
ACS Omega 2023, 8, 15141−15151